


Cite this: *RSC Adv.*, 2017, 7, 19345

Preparation of Ni(OH)₂ nanoplatelet/electrospun carbon nanofiber hybrids for highly sensitive nonenzymatic glucose sensors†

Linlin Chen, Lijuan Liu, Qiaohui Guo, * Zhonghui Wang, Guiling Liu, Shuiliang Chen and Haoqing Hou*

Ni(OH)₂ nanoplatelet/electrospun carbon nanofiber (ECF) hybrids have been simply prepared for the construction of nonenzymatic glucose biosensors. The resulting Ni(OH)₂/ECF hybrids were carefully examined using SEM, TEM, HRTEM, XRD, and XPS. For all hybrids, two-dimensional Ni(OH)₂ nanoplatelets were uniformly anchored on the one-dimensional ECFs, forming a hierarchical nanostructure, and the thickness of Ni(OH)₂ nanoplatelets could be readily tailored by controlling the content of Ni(OH)₂ precursor. Cyclic voltammetric studies showed enhanced redox properties for Ni(OH)₂/ECF-based electrodes relative to pure Ni(OH)₂ nanoplatelet electrode and significantly improved the electrocatalytic activity for glucose oxidation. The application of Ni(OH)₂/ECF-based electrodes to glucose detection was explored. A low limit of detection (0.1 μM), wide detection linear range (0.005–13.05 mM), and excellent signal stability and reproducibility were demonstrated by this novel Ni(OH)₂/ECF-0.06 hybrid. The sensor was also applied in real serum samples, giving satisfactory results. The simple preparation, low cost, and enhanced electrocatalytic performance of these hybrids could pave the way for highly sensitive glucose sensors.

Received 19th February 2017
Accepted 21st March 2017

DOI: 10.1039/c7ra02064c

rsc.li/rsc-advances

1 Introduction

Diabetes, a common chronic disease, is becoming an increasing threat to human health. In the last few years, considerable effort has been devoted to developing reliable and efficient methods for monitoring glucose in human blood, such as high-performance liquid chromatography method,¹ colorimetry,² chemiluminescence,³ electrochemiluminescence,⁴ and electrochemical sensors.^{5–7} Among these techniques, electrochemical biosensors are among the most convenient and promising due to their simplicity, rapid response, and high sensitivity.^{8,9} Electrochemical biosensors for glucose determination are commonly classified as enzymatic or nonenzymatic glucose sensors. Enzymatic glucose sensors, based on the immobilization of glucose oxidase (GOD) on various substrates, have been the subject of most previous studies in this field.¹⁰ Although these glucose sensors provide excellent selectivity and sensitivity, GOD-based biosensors suffer from intrinsic drawbacks, such as poor reproducibility, thermal and chemical instability, and high cost,¹¹ which limit their practical applications.

Nonenzymatic sensors have high sensitivity, long-term stability, rapid response times, and are low cost. They have received increasing attention as attractive alternatives for overcoming the limitations of enzymatic biosensors. Continuous research efforts towards the development of nonenzymatic sensors have culminated in the realization of electrocatalytic oxidation of glucose on bare metal surfaces. Early studies showed that glucose oxidation on some noble metals, such as Pt and Au, suffered from slow kinetics and were unable to generate significant faradaic current.¹² Moreover, noble metal surfaces are easily poisoned by adsorbed intermediates and chloride ions, leading to decreased sensitivity. Therefore, the search for novel materials with appropriate architectures is key for the fabrication of highly sensitive nonenzymatic glucose sensors. To address this problem, various transition metal oxides or metal hydroxides, such as NiO,¹³ CuO,¹⁴ Co₃O₄ (ref. 15) and Ni(OH)₂,¹⁶ have been reported as viable candidates. Among these relatively low cost materials, nanostructures of Ni(OH)₂, an important transition metal hydroxide, are promising candidates for active electrode materials in nonenzymatic glucose electrochemical sensors.

Various Ni(OH)₂-based nano/microstructures with enhanced electrochemical performance, such as nanoplatelets,¹⁷ nanoflakes,¹⁸ nanorods,¹⁹ nanoribbons,²⁰ nanowires,²¹ nanotubes,²² nanospheres,²³ and hollow microspheres²⁴ have been explored. Among them, nanoplatelets are deserving of attention in biosensor fabrication due to their interesting properties, such

Department of Chemistry and Chemical Engineering, Jiangxi Normal University, Nanchang, Jiangxi 330022, China. E-mail: guoqiaohui@jxnu.edu.cn; Fax: +86-791-8812-0536; Tel: +86-791-8812-0389

† Electronic supplementary information (ESI) available. See DOI: 10.1039/c7ra02064c



as large surface-to-volume ratio, well-defined interior void, and high specific surface area. Furthermore, decorating these $\text{Ni}(\text{OH})_2$ nanostructures onto the carbon substrate is a popular strategy for developing efficient sensors. The synergistic effect of $\text{Ni}(\text{OH})_2$ and the carbon substrate on which they were grown can result in enhanced sensing properties.

In this study, the prominent conductivity of electrospun carbon nanofibers (ECF) and electrocatalysis of $\text{Ni}(\text{OH})_2$ nanoplatelets were combined to construct a highly sensitive non-enzymatic glucose sensor based on an $\text{Ni}(\text{OH})_2$ /ECF hybrid. Fabrication of the $\text{Ni}(\text{OH})_2$ /ECF hybrid was cost-effective, time-saving, and scalable using a microwave-assisted method. The morphologies and structures of the $\text{Ni}(\text{OH})_2$ /ECF hybrids were characterized, and their electrochemical properties investigated in detail. Furthermore, $\text{Ni}(\text{OH})_2$ /ECF was successfully applied to glucose detection in real serum samples.

2 Experimental

2.1 Reagents

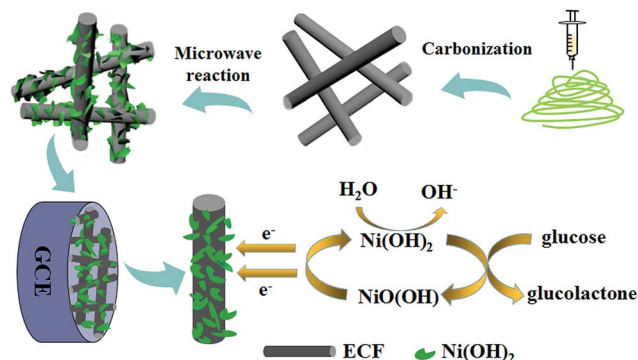
Polyacrylonitrile (PAN), nickel nitrate hexahydrate ($\text{Ni}(\text{NO}_3)_2 \cdot 6\text{H}_2\text{O}$), urea ($\text{CO}(\text{NH}_2)_2$), glucose, uric acid (UA), dopamine (DA) and ascorbic acid (AA) were purchased from Sigma-Aldrich Chemical Co. (St. Louis, MO, USA). All other reagents were of analytical grade and used without further purification.

2.2 Apparatus

Morphological characterization was performed using scanning electron microscopy (SEM; TESCAN VEGA-3) and transmission electron microscopy (TEM; Tecnai G20). The crystal structure was characterized by X-ray diffraction (XRD; Bruker D8 Advance diffractometer) and X-ray photoelectron spectroscopy (XPS; PHI Quantera). XPS data were collected using a dual anode X-ray source with Mg K radiation at an energy of 1253.6 eV. The microwave oven was used in the power range 0–1000 W (MAS-IIPlus model, Sine Microwave Chemical Technology Co., Ltd, China). The specific surface area and pore size distribution were measured using a Brunauer–Emmett–Teller (BET) analyzer. All electrochemical experiments were performed on a CHI 760 E electrochemical workstation (Shanghai, China). A three-electrode configuration was used, comprising a platinum wire as the auxiliary electrode, a Ag/AgCl (saturated KCl) reference electrode, and a bare glass carbon electrode (GC) or modified GC electrode as the working electrode. Electrochemical impedance spectroscopy (EIS) was performed in a 0.1 M KCl solution containing 10 mM $\text{Fe}(\text{CN})_6^{3-/4-}$ (1 : 1) as a supporting electrolyte at its open circuit potential, with a frequency range of 1.0×10^{-2} to 1.0×10^5 Hz, using an alternating current voltage of 5 mV.

2.3 Preparation of $\text{Ni}(\text{OH})_2$ /ECF hybrids

$\text{Ni}(\text{OH})_2$ /ECF was synthesized using a microwave method with ECF as the substrate.^{25,26} ECF film was prepared by combining electrospinning and subsequent carbonization. The general preparation was as follows: electrospun nanofibers were prepared using an electrospinning process performed in an electric field of 100 kV m^{-1} , created by applying a 30 kV



Scheme 1 Construction procedure for $\text{Ni}(\text{OH})_2$ /ECF sensor.

electrical potential to a 30 cm gap between the spinneret and collector. A PAN polymer solution (8 wt%) was prepared for nanofiber electrospinning. Oxidation of the electrospun nanofibers was performed in a tubular stainless steel reactor by oxidation of the precursor nanofibers at 250°C in air for 3 h, and then carbonized at 1100°C in a conventional tube furnace under a N_2 atmosphere. After cooling to room temperature, the as-prepared ECF was dipped into nitric acid for 1 h to attach hydrophilic groups. $\text{Ni}(\text{OH})_2$ /ECF hybrids with different loadings of $\text{Ni}(\text{OH})_2$ nanoplatelets on the ECF were prepared using a microwave method. Typically, a certain concentration of $\text{Ni}(\text{NO}_3)_2 \cdot 6\text{H}_2\text{O}$ (0.03, 0.06 or 0.12 M) and urea (2.88 g) were dissolved in distilled water (200 mL) and ethanol (20 mL) in a 500 mL three-necked flask in a microwave reactor. After stirring for approximately 30 min, the flexible ECF was carefully soaked in the solution followed by heating to 90°C for 20 min under microwave irradiation. After cooling to room temperature, the sample was washed with distilled water and absolute ethanol several times. $\text{Ni}(\text{OH})_2$ /ECF was then dried in a vacuum oven at 80°C for 24 h. The obtained $\text{Ni}(\text{OH})_2$ /ECF hybrids prepared using $\text{Ni}(\text{NO}_3)_2 \cdot 6\text{H}_2\text{O}$ concentrations of 0.03, 0.06, and 0.12 M were denoted as $\text{Ni}(\text{OH})_2$ /ECF-0.03, $\text{Ni}(\text{OH})_2$ /ECF-0.06, and $\text{Ni}(\text{OH})_2$ /ECF-0.12, respectively. For the control experiment, pure $\text{Ni}(\text{OH})_2$ nanoplatelets were synthesized *via* the same method without ECF addition.

2.4 Electrode preparation

The glass carbon electrode (GC, $\theta = 3 \text{ mm}$) was polished carefully using Al_2O_3 powder and rinsed and sonicated twice in distilled water before use in subsequent experiments. $\text{Ni}(\text{OH})_2$ /ECF (10 mg mL^{-1}) was dispersed in a mixture of Nafion (25 μL , 5 wt%) and distilled water (250 μL) by sonication. Immediately after dispersion, the $\text{Ni}(\text{OH})_2$ /ECF slurry (3 μL) was coated onto the GC electrode surface ($\text{Ni}(\text{OH})_2$ /ECF/GC) and dried at 25°C for 24 h. The procedure for $\text{Ni}(\text{OH})_2$ /ECF sensor fabrication is shown in Scheme 1.

3 Results and discussion

3.1 Characterization

To obtain $\text{Ni}(\text{OH})_2$ /ECF hybrids, an efficient microwave-assisted synthesis technique was utilized for the *in situ* growth of



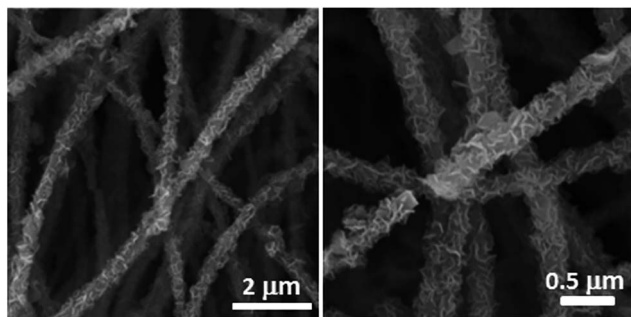


Fig. 1 SEM images of Ni(OH)₂/ECF-0.06.

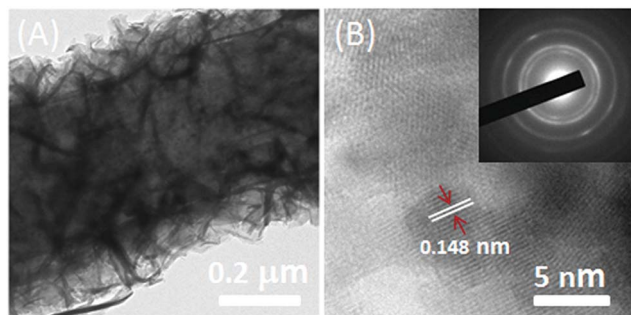


Fig. 2 (A) TEM and (B) HRTEM images and SAED pattern (inset) of Ni(OH)₂/ECF-0.06 hybrid.

crystallized Ni(OH)₂ nanoplatelets. Thin Ni(OH)₂ nanoplatelets with thicknesses of 60–150 nm were uniformly distributed throughout the ECF surface, which effectively prevented the

aggregation of Ni(OH)₂ nanoplatelets (Fig. 1). Furthermore, the Ni(OH)₂ nanoplatelet loading on ECF clearly increased with increasing Ni(NO₃)₂ concentration from 0.03 to 0.12 M. When the Ni(NO₃)₂ concentration was 0.03 M, the ECFs were not fully covered with Ni(OH)₂ nanoplatelets (Fig. S1A and B†). By increasing the concentration to 0.06 M, Ni(OH)₂ nanoplatelets with curled shapes became homogeneously distributed throughout the ECF surface (Fig. 1). However, a higher Ni(NO₃)₂ concentration of 0.12 M resulted in the accumulation of dense Ni(OH)₂ nanoplatelets, which formed a thick layer on the ECF surface (Fig. S1C and D†). This layer might deteriorate electron transfer between Ni(OH)₂ nanoplatelet sheath and ECF core. Therefore, better interfacial interactions between ECFs and Ni(OH)₂ nanoplatelets were achieved in the Ni(OH)₂/ECF-0.06 hybrid.

TEM analysis (Fig. 2A) revealed that Ni(OH)₂ nanoplatelets with thicknesses of 60 ± 6 nm had grown uniformly on the ECF surface, in good agreement with the SEM results (Fig. 1). The HRTEM image of Ni(OH)₂ nanoplatelets (Fig. 2B) exhibited well-defined lattice fringes, with lattice spacing of 0.148 nm, corresponding to the (110) plane of Ni(OH)₂. The corresponding SAED pattern (inset of Fig. 2B) showed diffuse rings, indicating that the Ni(OH)₂ nanoplatelets were polycrystalline. As mentioned above, 3D hierarchical nanostructures were constructed from two-dimensional (2D) Ni(OH)₂ nanoplatelets anchored on one-dimensional (1D) ECFs, which can effectively prevent the aggregation of Ni(OH)₂ nanoplatelets and might facilitate electrolyte diffusion to the electrochemically active of Ni(OH)₂ nanoplatelets.

The crystal structure of Ni(OH)₂/ECF-0.06 was studied by XRD. The Ni(OH)₂/ECF hybrid displayed four diffraction peaks

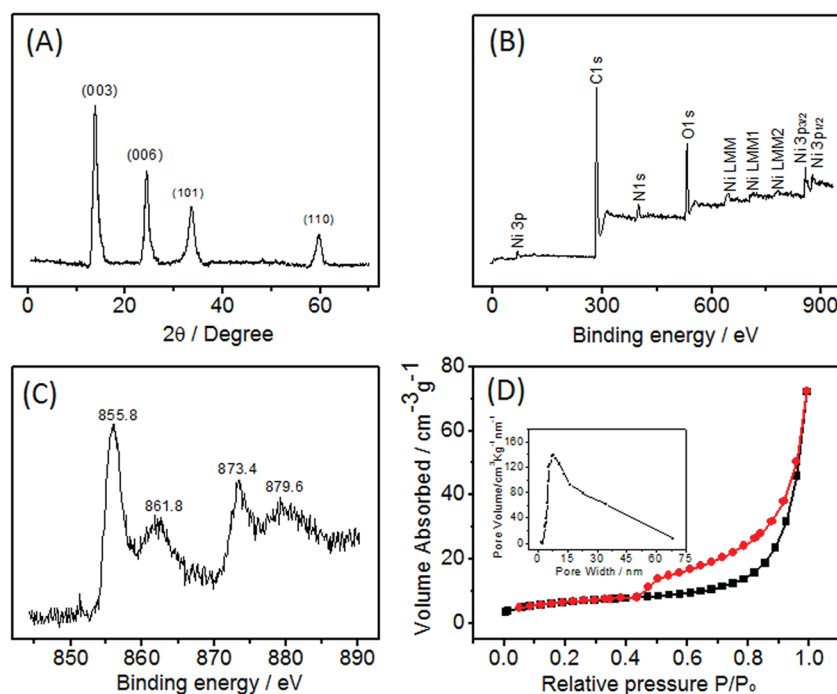


Fig. 3 (A) XRD pattern, (B) XPS survey spectrum, (C) high-resolution Ni 2p spectrum, and (D) nitrogen adsorption–desorption isotherms of Ni(OH)₂/ECF-0.06 hybrid. Inset: pore size distribution calculated using the Barrett–Joyner–Halenda (BJH) method.



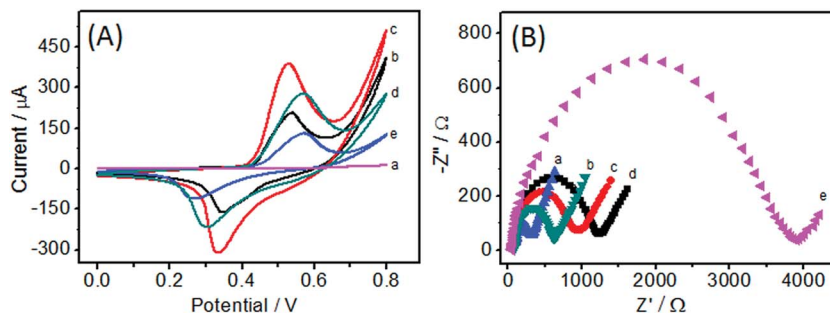


Fig. 4 (A) CV curves and (B) Nyquist plots of (a) ECF, (b) $\text{Ni(OH)}_2/\text{ECF}-0.03$, (c) $\text{Ni(OH)}_2/\text{ECF}-0.06$, (d) $\text{Ni(OH)}_2/\text{ECF}-0.12$ and (e) pure Ni(OH)_2 nanoplatelets in 0.1 M NaOH solution, using a scan rate of 50 mV s^{-1} .

at $2\theta = 13.8^\circ$, 25.9° , 35.8° , and 59.6° (Fig. 3A), corresponding to the (003), (006), (101), and (110) planes of Ni(OH)_2 (JCPDS 38-0715), respectively. No peaks were detected for NiO or Ni, indicating that Ni(OH)_2 had formed with good phase purity in the hybrid. The chemical state of the $\text{Ni(OH)}_2/\text{ECF}-0.06$ hybrid was further investigated by XPS analysis. The XPS survey spectrum revealed the presence of C, Ni, and O in $\text{Ni(OH)}_2/\text{ECF}-0.06$ (Fig. 3B). The high-resolution spectrum of Ni 2p (Fig. 3C) showed two main peaks at 855.8 and 873.4 eV, corresponding to Ni 2p_{3/2} and Ni 2p_{1/2}, respectively. Furthermore, their associated satellite peaks, located at 864.8 eV (Ni 2p_{3/2}, satellite) and 879.6 eV (Ni 2p_{1/2}, satellite), were also observed, which were typical characteristics of the Ni(OH)_2 phase, in good agreement with previous reports.²⁷

The nitrogen adsorption-desorption isotherm curve showed a type-IV isotherm (Fig. 3D), with a sharp capillary condensation step at a relatively high pressure, implying the presence of a porous structure and a narrow pore size distribution, in agreement with the SEM and TEM results. The calculated specific surface area of $\text{Ni(OH)}_2/\text{ECF}-0.06$ was $125.2 \text{ m}^2 \text{ g}^{-1}$. The pore size distribution was calculated using the BJH method (Fig. 3D, inset). The pore diameter was mainly distributed at around 8–12 nm with a large pore volume. A high surface area and uniform pore distribution are especially beneficial for Ni(OH)_2 -based sensing because these properties promote interactions between electrolyte and material, and allow for the high accessibility of target molecules to electrode surface.²⁸

3.2 Electrochemical behavior of $\text{Ni(OH)}_2/\text{ECF}$ hybrids

To understand the electrochemical properties of $\text{Ni(OH)}_2/\text{ECF}$ hybrids, cyclic voltammetry (CV) analysis was performed in 0.1 M NaOH solution. All $\text{Ni(OH)}_2/\text{ECF}$ modified electrodes had pairs of redox peaks in the potential range 0.25–0.55 V, corresponding to the $\text{Ni(II)}/\text{Ni(III)}$ redox couple in alkaline medium (Fig. 4A). In comparison with pure Ni(OH)_2 nanoplatelet modified electrode, $\text{Ni(OH)}_2/\text{ECF}$ exhibited lower anodic peak potentials and enhanced redox currents (Fig. 4A, curves b–d), indicating that $\text{Ni(II)}/\text{Ni(III)}$ redox processes were facilitated in the $\text{Ni(OH)}_2/\text{ECF}$ hybrids. The $\text{Ni(OH)}_2/\text{CNF}-0.06$ modified electrode showed the lowest anodic peak potential of approx. 0.42 V and the highest peak currents among the $\text{Ni(OH)}_2/\text{ECF}$ modified electrodes (Fig. 4A, curve c), suggesting a high redox activity. The control experiment of the ECF-modified electrode displayed no redox peak during the potential scan (Fig. 4A, curve a).

To better understand the superior electrochemical properties of $\text{Ni(OH)}_2/\text{ECF}$ hybrids, EIS was carried out. Electron transfer resistance (R_{ct}), which is known to dictate the electron transfer kinetics of the redox probe at the electrode interface, was measured using EIS (Fig. 4B). The R_{ct} values of $\text{Ni(OH)}_2/\text{ECF}$ modified electrodes (Fig. 4B, curves b–d) were smaller than that of the pure Ni(OH)_2 nanoplatelet modified electrode (Fig. 4B, curves e), suggesting that the ECF matrix significantly enhanced the electrical conductivity of the $\text{Ni(OH)}_2/\text{ECF}$ hybrids.

3.3 Electrocatalytic oxidation of glucose

Ni(OH)_2 -based nanomaterials have been reported to show excellent catalytic ability toward some electroactive molecules, including glucose,²⁹ ethanol,³⁰ and amino acids.³¹ Herein, the good electrochemical performance of ECF, including high electrical conductivity and large surface area, was expected to be combined with the electrocatalytic activity of Ni(OH)_2 nanoplatelets toward glucose oxidation. Fig. 5 and S2† show CV curves of $\text{Ni(OH)}_2/\text{ECF}$ and pure Ni(OH)_2 nanoplatelet modified electrodes with various glucose concentrations in 0.1 M NaOH solution. Upon addition of 50.0, 100.0, and 200.0 μM glucose, $\text{Ni(OH)}_2/\text{ECF}$ modified electrodes exhibited a substantial increase in both anodic and cathodic peak currents at around 0.55 V and 0.25 V, respectively, and a positive shift in the anodic peak potential by around 0.02 V (Fig. 5 and S2†). Additionally,

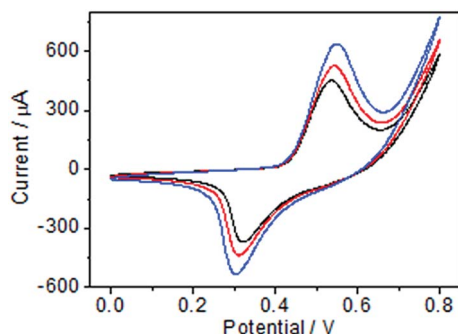


Fig. 5 CV curves of $\text{Ni(OH)}_2/\text{ECF}-0.06$ modified electrode in 0.1 M NaOH solution containing glucose concentrations of 50 μM (black line), 100 μM (red line), and 200 μM (blue line) at a scan rate of 50 mV s^{-1} .



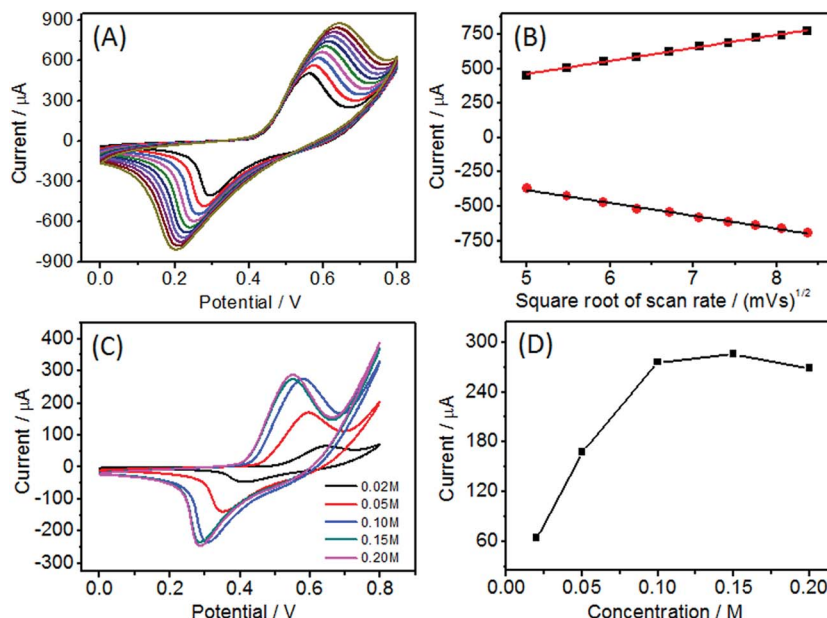


Fig. 6 (A) CV curves of Ni(OH)₂/ECF-0.06 at different scan rates from 25 to 70 mV s⁻¹ (inside to outside: 25 to 70 mV s⁻¹) in 0.1 M NaOH solution and (C) in NaOH concentrations of 0.02–0.20 M containing 2.0 mM glucose. (B) Plots of anodic and cathodic peak currents versus the square root of the scan rate. (D) Calibration curves of peak current versus NaOH concentration.

the catalytic currents of Ni(OH)₂/ECF modified electrodes were markedly larger than that of the pure Ni(OH)₂ nanoplatelet modified electrode, indicating enhanced electrocatalytic activity for the Ni(OH)₂/ECF hybrids, which might be attributed to the synergistic effect of well-dispersed Ni(OH)₂ and ECF, and the increased hybrid conductivity and surface area. The electro-oxidation of glucose at Ni(OH)₂/ECF modified electrodes can be described as follows:³²



Glucose was oxidized by NiOOH species on the electrode surface under the anodic potential, which converted the NiOOH species to Ni(OH)₂.

3.4 Effects of scan rate and NaOH concentration

The influence of scan rate on Ni(OH)₂/ECF-0.06 was investigated in 0.1 M NaOH solution containing 1.0 mM glucose. The peak currents for both anodic and cathodic peaks were proportional to the square root of the scan rate (Fig. 6A and B). The results indicated that the electrochemical kinetics at the Ni(OH)₂/ECF-0.06 modified electrode surface were diffusion-controlled.

Hydroxide concentration played an important role in glucose oxidation on Ni(OH)₂/ECF-0.06 due to the dehydrogenation of gluconolactone. As shown in Fig. 6C and D, the response increased with increasing NaOH concentration, from 0.02 to 0.10 M. Afterwards the response increased slowly as the concentration further increased in the range 0.10–0.20 M. Therefore, 0.10 M NaOH solution was chosen as the supporting electrolyte solution.

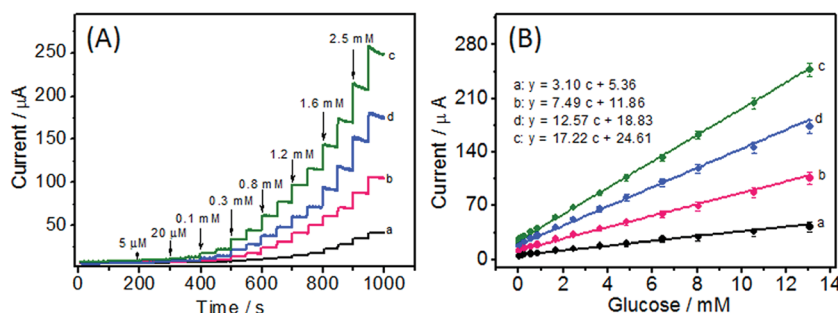


Fig. 7 (A) Amperometric responses of (a) pure Ni(OH)₂ nanoplatelet modified electrodes, (b) Ni(OH)₂/ECF-0.03, (c) Ni(OH)₂/ECF-0.06 and (d) Ni(OH)₂/ECF-0.12 upon successive addition of different glucose concentrations to 0.1 M NaOH solution at +0.55 V. (B) Plots of current versus corresponding glucose concentration.

Table 1 Comparison of Ni(OH)₂/ECF-0.06 sensor performance with other Ni(OH)₂-based nonenzymatic glucose sensors

Electrode materials	Sensitivity ($\mu\text{A cm}^{-2} \text{mM}^{-1}$)	Linear range (mM)	Detection limit (μM)	References
RGO-Ni(OH) ₂ /GCE	11.43	0.002–3.1	0.6	18
PI/CNT-Ni(OH) ₂	2071.5	0.001–0.8	0.36	19
Ni(OH) ₂ /ERGO ^a -MWNT/GC	2042	0.05–1.5	2.7	20
NiCFP ^b	420.4	0.002–2.5	1.0	33
Ni(OH) ₂ /NPGF ^c	2650	0.001–1.17	0.34	34
Ni(OH) ₂ /3DGF ^d	3529	0.002–7.0	0.73	35
Ni(OH) ₂ /nanoflowers	265.3	0.1–1.1	0.5	36
Ni(OH) ₂ /TiO ₂	192.5	0.03–14	8.0	37
Ni(OH) ₂ NP/MoS _x	162	0.01–1.3	5.8	38
α -Ni(OH) ₂ NP/FIA ^e	446	0.01–0.75	3.0	39
Pt-NiO/rGO	832.95	0.008–14.5	2.67	40
Ni(OH) ₂ /ECF	1342.2	0.005–13.05	0.1	This work

^a Electroreduced graphene oxide. ^b Ni nanoparticle-loaded carbon nanofiber paste electrode. ^c Nanoporous gold film. ^d Three-dimensional graphene foam. ^e Chemical bath deposited hollow Ni(OH)₂ nanorod arrays.

3.5 Amperometric detection of glucose

Nonenzymatic glucose sensors that take advantage of electrocatalytic glucose oxidation are of great research interest. Given the significant changes in redox current intensity of Ni(OH)₂/ECF upon addition of glucose, amperometric detection of glucose using Ni(OH)₂/ECF-based electrodes appears promising. Therefore, Ni(OH)₂/ECF hybrids were further evaluated for their amperometric responses to glucose. As shown in Fig. 7A, upon successive addition of various glucose concentrations, significant and quick responses were observed for all Ni(OH)₂/ECF modified electrodes with 95% of the steady-state current achievable within 3 s. In comparison, the Ni(OH)₂ modified electrode showed the lowest sensitivity among all electrodes tested. The Ni(OH)₂/ECF modified electrodes exhibited improved sensitivity relative to Ni(OH)₂ modified electrodes, which was attributed to the increased electrocatalytically active surface area resulting from the well dispersion of Ni(OH)₂ nanoplatelets in the ECF support. In general, the amperometric sensitivity of the tested electrodes was in the order Ni(OH)₂ < Ni(OH)₂/ECF-0.03 < Ni(OH)₂/ECF-0.12 < Ni(OH)₂/ECF-0.06 (Fig. 7B). The Ni(OH)₂/ECF-0.06 electrode showed the highest glucose sensitivity, which was more than three-fold greater than that of the Ni(OH)₂ modified electrode. The calibration plot of the Ni(OH)₂/CNF-0.06 electrode for

glucose detection could be obtained in a wide concentration range, from 5 μM to 13.05 mM ($R = 0.992$) with a limit of detection (LOD) of 0.1 μM ($S/N = 3$). The linear regression equation of the Ni(OH)₂/CNF-0.06 electrode for glucose detection was: $y (\mu\text{A}) = 17.22C + 24.61$ ($R = 0.992$). This wide linear range was superior to most state-of-the-art nonenzymatic glucose sensors, such as RGO-Ni(OH)₂/GCE,¹⁸ Ni(OH)₂/ERGO-MWNT/GC,²⁰ and Ni(OH)₂/nanoflower electrodes.³⁶ The performance of the Ni(OH)₂/ECF-0.06 sensor is compared with other Ni(OH)₂-based nonenzymatic glucose sensors in Table 1.

3.6 Selectivity of Ni(OH)₂/ECF-0.06

To further explore Ni(OH)₂/ECF-0.06 as a reliable platform for enzyme-free glucose sensing, practical testing conditions must be taken into consideration. In real samples, some electrochemically active substances, such as ascorbic acid (AA), uric acid (UA), dopamine (DA), and some sugars with similar chemical structures, might cause interference. The normal physiological level of glucose is about 3.0–8.0 mM in human serum, while levels of carbohydrates, such as xylose, mannose, lactose, and maltose, and AA, DA, and UA, are about 0.1 mM.²⁶ A well-defined glucose response was obtained, while insignificant responses were observed for interfering species (Fig. 8A).

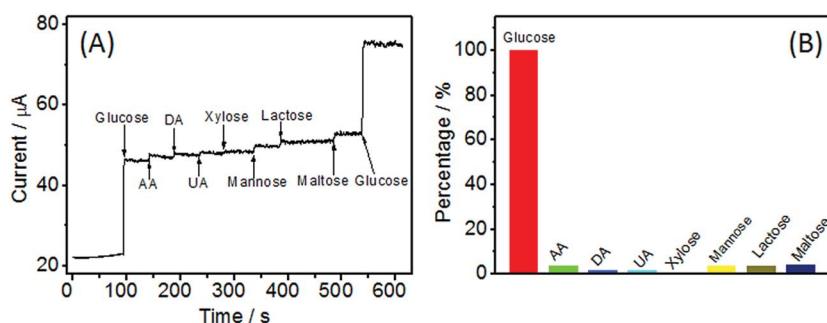


Fig. 8 (A) Interference test for Ni(OH)₂/ECF-0.06 modified electrode in 0.1 M NaOH at +0.55 V with 1.0 mM glucose and other interferents, including AA, DA, UA, xylose, mannose, lactose, and maltose (all 0.1 mM). (B) Interfering signal percentages compared with glucose.



Table 2 Determination of glucose in human serum samples ($n = 6$)

Sample	Proposed sensor (mM)	Glucometer (mM)	Added (mM)	Found (mM)	Recovery (%)
1	4.45	4.52	0.50	4.92	98.5
2	4.42	4.31	1.0	5.42	102.6
3	4.50	4.51	1.5	5.98	99.3

Compared with glucose, the current responses were 3.85%, 1.87%, 1.70%, 0.85%, 2.93%, 3.32%, and 3.31% for AA, DA, UA, xylose, mannose, lactose, and maltose, respectively (Fig. 8B). Therefore, Ni(OH)₂/ECF-0.06 showed satisfactory selectivity for glucose detection in the presence of potential interfering reagents.

Given that many metal-based glucose sensors are susceptible to chloride ion poisoning, the antifouling ability of the Ni(OH)₂/ECF-0.06 electrode was probed by performing i - t measurements in 0.1 M NaOH (aq.) containing 1 M NaCl. No changes in the current responses of Ni(OH)₂/ECF-0.06 to glucose were discernible (Fig. S3†), confirming the good resistance to surface fouling.

3.7 Reproducibility and analysis of real samples

The reproducibility of the Ni(OH)₂/ECF-0.06 modified electrode was estimated from the current response of six different electrodes to 2.0 mM glucose. The RSD was calculated as 3.35%. Furthermore, the Ni(OH)₂/ECF-0.06 modified electrode showed an RSD of 3.55% for six successive measurements of 5.0 mM glucose, demonstrating that Ni(OH)₂/ECF-0.06 was stable and suitable for repeated glucose detection. The long-term stability of this modified electrode was tested after storing at room temperature for one month, and no significant change in current response was observed, implying that the biosensor could be used in long-term routine applications.

To verify that the sensor can be applied in clinical diagnostics, the as-fabricated sensor was used to determine the glucose concentration of human blood serum. Human serum samples were received from Nanchang People's Hospital without any pretreatment. The glucose contents measured using the proposed method were in good agreement with data provided by the glucometer (Sejong Biotechnology Co., China) (Table 2). Meanwhile, the recovery was 98.5–102.6% with an RSD below 3.05%, suggesting the strong applicability of the sensor to real samples.

4 Conclusions

In summary, Ni(OH)₂/ECF hybrids comprising Ni(OH)₂ nanoplatelets uniformly grown on electrospun carbon nanofibers were simply prepared and used as nonenzymatic glucose biosensing electrode materials. ECFs have good electrical conductivity, which not only facilitated charge transfer across the interfaces for fast redox reactions of Ni(OH)₂ nanoplatelets, but also effectively mitigated their aggregation. Moreover, the hierarchical nanostructures of Ni(OH)₂/ECF provided

continuous channels, which enabled rapid electrolyte diffusion to access the electrochemically active Ni(OH)₂ nanoplatelets. Benefiting from these synergistic effects, Ni(OH)₂/ECF presented excellent nonenzymatic glucose sensing performance in terms of sensitivity, selectivity, response time, and linear calibration. This strategy provides a new, reliable, effective, and promising method for the application of Ni(OH)₂/ECF hybrids in high-performance glucose sensing.

Acknowledgements

This work was financially supported by the National Natural Science Foundation of China (21405065) and the Science and Technology Project of Jiangxi Province (20161BCB24005).

Notes and references

- 1 S. Song, L. Sun, L. Yuan, T. Sun, Y. Zhao, W. Zuo, Y. Cong, X. Li and J. Wang, *J. Chromatogr. A*, 2008, **1179**, 125–130.
- 2 D. Nakayama, Y. Takeoka, M. Watanabe and K. Kataoka, *Angew. Chem.*, 2003, **115**, 4329–4332.
- 3 Y. Lv, Z. Zhang and F. Chen, *Talanta*, 2003, **59**, 571–576.
- 4 C. A. Marquette, A. Degiuli and L. C. J. Blum, *Biosens. Bioelectron.*, 2003, **19**, 433–439.
- 5 P. Lu, S. Liu, G. Dai, Y. Lei and Y. Liang, *Aust. J. Chem.*, 2013, **66**, 983–988.
- 6 L. Gorton, G. Bremle, E. Csöregi, G. Jönsson-Pettersson and B. Persson, *Anal. Chim. Acta*, 1991, **249**, 43–54.
- 7 J. Wang and M. Musameh, *Anal. Chim. Acta*, 2005, **539**, 209–213.
- 8 S. Duan, X. Zhang, S. Xu and C. Zhou, *Electrochim. Acta*, 2013, **88**, 885–891.
- 9 W. X. Zhang, J. Z. Zheng, J. G. Shi, Z. Q. Lin and Q. T. Huang, *Anal. Chim. Acta*, 2015, **853**, 285–290.
- 10 R. Wilson and A. P. F. Turner, *Biosens. Bioelectron.*, 1992, **7**, 165–185.
- 11 Q. Yan, Z. Wang, J. Zhang, H. Peng, X. Chen, H. Hou and C. Liu, *Electrochim. Acta*, 2012, **61**, 148–153.
- 12 Y. Li, Y. Y. Song, C. Yang and X. H. Xia, *Electrochem. Commun.*, 2007, **9**, 981–988.
- 13 Y. Mu, D. Jia, Y. He, Y. Miao and H. L. Wu, *Biosens. Bioelectron.*, 2011, **26**, 2948–2952.
- 14 L. C. Jiang and W. D. Zhang, *Biosens. Bioelectron.*, 2010, **25**, 1402–1407.
- 15 L. J. Ding, M. G. Zhao, S. S. Fan, Y. Ma, J. J. Liang, X. T. Wang, Y. W. Song and S. G. Chen, *Sens. Actuators, B*, 2016, **235**, 162–169.
- 16 Y. Zhang, F. G. Xu, Y. J. Sun, Y. Shi, Z. W. Wen and Z. Li, *J. Mater. Chem.*, 2011, **21**, 16949–16954.
- 17 H. Wang, H. S. Casalongue, Y. Liang and H. Dai, *J. Am. Chem. Soc.*, 2010, **132**, 7472–7477.
- 18 J. W. Lang, L. B. Kong, W. J. Wu, M. Liu, Y. C. Luo and L. Kang, *J. Solid State Electrochem.*, 2009, **13**, 333–340.
- 19 J. H. Liang and Y. Li, *ChemInform*, 2004, **35**, 134–138.
- 20 D. N. Yang, R. M. Wang, J. Zhang and Z. F. Liu, *J. Phys. Chem. B*, 2004, **108**, 7531–7533.



- 21 H. Jiang, C. Li, T. Sun and J. Ma, *Chem. Commun.*, 2012, **48**, 2606–2608.
- 22 L. Zhuo, J. Ge, L. Cao and B. Tang, *Cryst. Growth Des.*, 2009, **9**, 1–6.
- 23 D. B. Kuang, B. X. Lei, Y. P. Pan, X. Y. Yu and C. Y. Su, *J. Phys. Chem. C*, 2009, **113**, 5508–5513.
- 24 L. P. Zhu, G. H. Liao, Y. Yang, H. M. Xiao, J. F. Wang and S. Y. Fu, *Nanoscale Res. Lett.*, 2009, **4**, 550–557.
- 25 G. Y. Zhou, T. R. Xiong, S. J. He, Y. H. Li, Y. M. Zhu and H. Q. Hou, *J. Power Sources*, 2016, **317**, 57–64.
- 26 L. S. Zhang, Q. W. Ding, Y. P. Huang, H. H. Gu, Y. E. Miao and T. X. Liu, *ACS Appl. Mater. Interfaces*, 2015, **7**, 22669–22677.
- 27 H. Chen, S. X. Zhou and L. M. Wu, *ACS Appl. Mater. Interfaces*, 2014, **6**, 8621–8630.
- 28 A. Walcarius, *Chem. Soc. Rev.*, 2013, **42**, 4098–4140.
- 29 Q. H. Guo, D. Liu, X. P. Zhang, L. B. Li, H. Q. Hou, O. Niwa and T. Y. You, *Anal. Chem.*, 2014, **86**, 5898–5905.
- 30 Y. Liu, L. Zhang, Q. H. Guo, H. Q. Hou and T. Y. You, *Anal. Chim. Acta*, 2010, **663**, 153–157.
- 31 Z. B. Chen, J. W. Nai, H. Ma and Z. Q. Li, *Electrochim. Acta*, 2014, **116**, 258–262.
- 32 G. Wang, X. Lu, T. Zhai, Y. Ling, H. Wang and Y. Tong, *Nanoscale*, 2012, **4**, 3123–3130.
- 33 Y. Liu, H. Teng, H. Q. Hou and T. Y. You, *Biosens. Bioelectron.*, 2009, **24**, 3329–3334.
- 34 B. B. Zhan, C. B. Liu, H. P. Chen, H. X. Shi, L. H. Wang, P. Chen, W. Huang and X. C. Dong, *Nanoscale*, 2014, **6**, 7424–7429.
- 35 M. M. Guo, X. L. Yin, C. H. Zhou, Y. Xia, W. Huang and Z. L. Li, *Electrochim. Acta*, 2014, **142**, 351–358.
- 36 H. P. Yang, G. W. Gao, F. Teng, W. J. Liu, S. J. Chen and Z. C. Ge, *J. Electrochem. Soc.*, 2014, **161**, B216–B219.
- 37 A. Gao, X. M. Zhang, X. Peng, H. Wu, L. Bai, W. H. Jin, G. S. Wu, R. Q. Hang and P. K. Chu, *Sens. Actuators, B*, 2016, **232**, 150–157.
- 38 S. Ji, Z. Yang, C. Zhang, Y. E. Miao, W. W. Tjiu, J. Pan and T. X. Liu, *Microchim. Acta*, 2013, **180**, 1127–1134.
- 39 P. R. Martins, M. A. Rocha, L. Angnes, H. E. Toma and K. Araki, *Electroanalysis*, 2011, **23**, 2541–2548.
- 40 L. Wang, X. P. Lu, C. J. Wen, Y. Z. Xie, L. F. Mao, S. H. Chen, H. B. Li, P. Li and Y. H. Song, *J. Mater. Chem. A*, 2015, **3**, 608–616.

